

# Water-promoted interfacial pathways in methane oxidation to methanol on a CeO<sub>x</sub>-Cu<sub>2</sub>O catalyst

**Authors:** Zongyuan Liu<sup>1†</sup>, Erwei Huang<sup>2†</sup>, Ivan Orozco<sup>2</sup>, Wenjie Liao<sup>2</sup>, Robert M. Palomino<sup>1</sup>, Ning Rui,<sup>1</sup> Thomas Duchon<sup>3</sup>, Slavomir Nemsak<sup>4</sup>, David Grinter,<sup>5</sup> Mausumi Mahapatra<sup>1</sup>, Ping Liu<sup>1,2,\*</sup>, José A. Rodriguez<sup>1,2,\*</sup>, Sanjaya D. Senanayake<sup>1,\*</sup>

## Affiliations:

<sup>1</sup>Chemistry Division, Brookhaven National Laboratory, Upton, NY 11973 USA.

<sup>2</sup>Chemistry Department, Stony Brook University, Stony Brook, NY 11794 USA.

<sup>3</sup>Peter-Grünberg-Institut 6, Forschungszentrum Jülich, 52425 Jülich, Germany.

<sup>4</sup>Advanced Light Source, Lawrence Berkeley National Laboratory, Berkeley, CA 94720, USA.

<sup>5</sup>Diamond Light Source Limited, Diamond House, Harwell Science and Innovation Campus, Didcot, Oxfordshire OX11 0DE, U.K.

\*Correspondence to: [pingliu3@bnl.gov](mailto:pingliu3@bnl.gov) (P.L.); [rodrigez@bnl.gov](mailto:rodrigez@bnl.gov) (J.A.R.); [ssenanay@bnl.gov](mailto:ssenanay@bnl.gov) (S.D.S)

†Dr. Z. Liu and E. Huang contributed equally to this work and should be regarded as co-first authors.

**Abstract:** Highly selective oxidation of methane to methanol has long been challenging in catalysis. Here, we reveal key steps for the promotion by water when tuning the selectivity of a well-defined CeO<sub>x</sub>/Cu<sub>2</sub>O/Cu(111) catalyst from CO and CO<sub>2</sub> to methanol under a reaction environment with methane, oxygen and water. Ambient-pressure x-ray photoelectron spectroscopy showed that water added to CH<sub>4</sub> and O<sub>2</sub> led to surface CH<sub>3</sub>O and accelerated methanol production. These results were consistent with density functional theory calculations and kinetic Monte Carlo simulations which showed that water preferentially dissociates over the active Ce ions at the CeO<sub>2</sub>-Cu<sub>2</sub>O/Cu(111) interface. The adsorbed OH blocked O-O bond cleavage that would dehydrogenate CH<sub>3</sub>O to CO and CO<sub>2</sub>, and it directly converted this species to methanol, while O<sub>2</sub> now reoxidized the reduced surface. Water adsorption also displaced the produced methanol into the gas phase.

**One Sentence Summary:** New mechanistic insights on the role of water in the direct catalytic conversion of methane to methanol.

**Main Text:** Methane (CH<sub>4</sub>), the main component of natural gas, is difficult to upgrade to value added chemicals (aromatics, olefins, oxygenates) or even hydrogen (H<sub>2</sub>) because of its strong C-H bonds (104 kcal/mol). In nature, enzymes use oxygen-containing molecules such as water (H<sub>2</sub>O), oxygen (O<sub>2</sub>), and carbon dioxide (CO<sub>2</sub>) to convert CH<sub>4</sub> to methanol (CH<sub>3</sub>OH) at ambient temperature directly, unlike commercial process that require the energy-intensive formation of syngas (H<sub>2</sub> and CO) (1-4). Applying such biomimetic strategies to heterogeneous catalysts is often limited by the need for high temperatures that lead to poor selectivity (5-11), but some oxide and metal/oxide surfaces can dissociate CH<sub>4</sub> at room temperature, which opens the possibility for a direct CH<sub>4</sub> → CH<sub>3</sub>OH conversion (12-13). Indeed, a Ni/CeO<sub>2</sub>(111) catalyst can directly synthesize CH<sub>3</sub>OH on exposure to a mixture of CH<sub>4</sub>, O<sub>2</sub> and H<sub>2</sub>O. The selectivity of the process is rather low

(<40%) (14). On the other hand, an inverse catalyst of the CeO<sub>2</sub>/Cu<sub>2</sub>O/Cu(111) type displays a CH<sub>4</sub> to CH<sub>3</sub>OH selectivity close to 70% (16).

Extensive studies have investigated the reaction mechanism, including the active sites, the nature of reaction intermediates, the operating pathway and the role of O<sub>2</sub> and H<sub>2</sub>O in the CH<sub>4</sub> → CH<sub>3</sub>OH conversion. Some studies have proposed O<sub>2</sub> as the oxidizing agent for conversion of CH<sub>4</sub> to CH<sub>3</sub>O and CH<sub>3</sub>OH through the generation of an active metal=O species on the catalyst surface at high temperature (450 to 500 K) (10, 14, 17-19). H<sub>2</sub>O can help in the hydrogenation of CH<sub>3</sub>O or block surface sites preventing its decomposition and facilitating the extraction of methanol (10, 11, 14). In the case of Cu-containing zeolites that mimic enzymes, CH<sub>3</sub>OH generation is a sequential process that involves treatment or activation with O<sub>2</sub>, reaction with CH<sub>4</sub>, and finally extraction with water (6, 7, 11, 20). For the active CeO<sub>2</sub>/Cu<sub>2</sub>O/Cu(111) catalyst, the origin of the high selectivity (~ 70%) toward CH<sub>3</sub>OH remains elusive.

We combined ambient-pressure x-ray photoelectron spectroscopy (AP-XPS) with density functional theory (DFT) calculations and kinetic Monte Carlo (KMC) simulation and obtained direct evidence for the essential role of H<sub>2</sub>O in the selective production of CH<sub>3</sub>OH upon exposure of CH<sub>4</sub>, O<sub>2</sub> and H<sub>2</sub>O over the CeO<sub>2</sub>/Cu<sub>2</sub>O/Cu(111) catalyst. The spectroscopic measurement and theoretical modeling agreed that H<sub>2</sub>O acts not only as an extractor of CH<sub>3</sub>OH as previously reported (10, 11, 14), but more importantly as a blocker and active chemical reagent. The addition of H<sub>2</sub>O blocks the metal=O mediated mechanism proposed previously (10, 14, 17-19) and prevents the complete dissociation of CH<sub>4</sub> to form CO or CO<sub>2</sub>, and opens a new \*OH-mediated pathway, which enables the activation of CH<sub>4</sub> for direct CH<sub>3</sub>OH formation at the CeO<sub>2</sub>-Cu<sub>2</sub>O/Cu(111) interface. Direct CH<sub>4</sub> → CH<sub>3</sub>OH conversion by \*OH opens new opportunities to more active and selective catalysts for CH<sub>4</sub> utilization.

Both Cu-containing enzymes (3, 4) and zeolites (6, 10, 11) convert CH<sub>4</sub> into CH<sub>3</sub>OH. The oxidation state of the copper in these systems is usually assumed to be +2 before reaction with CH<sub>4</sub> and +1 after CH<sub>4</sub> activation (6). In AP-XPS experiments, we found a very low reactivity of plain Cu<sub>2</sub>O/Cu(111) systems toward CH<sub>4</sub> at room temperature. But this system and ceria are very active for water dissociation (15, 21). The deposition of cerium on Cu<sub>2</sub>O/Cu(111) under an atmosphere of O<sub>2</sub> (5 × 10<sup>-7</sup> torr) leads to formation of two types of islands, as shown by images of scanning tunneling microscopy (STM) (22). Large islands of ceria (30 to 50 nm in size and triangular shape) were embedded in the substrate step edges and had a morphology different from that seen for the two most stable surfaces of bulk ceria: CeO<sub>2</sub>(111) and CeO<sub>2</sub>(110) (22). These islands had a high of ~ 0.3 nm, which was consistent with a single layer of cerium sandwiched in between two layers of oxygen. In addition to the large ceria islands, a small concentration of small ceria islands formed that were 0.5 to 5 nm in size (16,22).

As shown in Fig. 1A, exposing a CeO<sub>x</sub>/Cu<sub>2</sub>O/Cu(111) surface (θ<sub>CeO<sub>2</sub></sub> = 0.5) to 20 mTorr of CH<sub>4</sub> at 300 K resulted in two peaks at ~287.0 eV and 285.3 eV in the C 1s region, which we attributed to the CH<sub>4</sub> gas phase and surface -CH<sub>x</sub> species, respectively (14). The formation of -CH<sub>x</sub> resulted from the dissociative adsorption of CH<sub>4</sub> at room temperature at a coverage of ~ 0.15 monolayer (ML). The hydrocarbon fragment had a relatively strong surface bond as it is still adsorbed on surface at 450 K. At this temperature, an additional feature grew in 289.4 eV that corresponded to CO<sub>x</sub> groups formed by the reaction between surface O sites and C atoms produced by the full decomposition of CH<sub>4</sub> (14). Thus, in contrast to plain Cu<sub>2</sub>O/Cu(111), the CeO<sub>2</sub>/Cu<sub>2</sub>O/Cu(111) surface exhibited substantial reactivity toward CH<sub>4</sub>.

The C 1s XPS acquired while exposing CuO<sub>2</sub>/Cu(111) and several CeO<sub>2</sub>/CuO<sub>2</sub>/Cu(111) surfaces to 20 mTorr of CH<sub>4</sub> at 300 K are compared in Fig. 1B. After normalization by the intensity of the peak for gaseous CH<sub>4</sub>, the most active CeO<sub>2</sub>/Cu<sub>2</sub>O/Cu(111) system was that with a ceria coverage near 0.5 ML (Fig. 1C). A 1.5 ML ceria system was not very active, probably because the ceria-copper oxide interface was substantially reduced and ceria deactivated when two-dimensional (2D) islands grew into three-dimensional (3D) ones (22). When these AP-XPS results are compared with data of catalytic activity for the conversion of CH<sub>4</sub> on CeO<sub>2</sub>/Cu<sub>2</sub>O/Cu(111) (16), one finds excellent agreement between the ability of the surface to activate CH<sub>4</sub> at room temperature and its activity for the conversion of the hydrocarbon to CH<sub>3</sub>OH or a CO/CO<sub>2</sub> mixture. A CeO<sub>2</sub>/Cu<sub>2</sub>O/Cu(111) system with 0.5 ML of ceria exhibited the best performance for CH<sub>4</sub> activation and conversion.

Over Cu-containing zeolites, CH<sub>3</sub>OH is produced by the sequential steps of activation in O<sub>2</sub>, reaction with CH<sub>4</sub> and extraction with H<sub>2</sub>O (6, 7, 11, 20). After sequentially adding 10 mTorr of O<sub>2</sub> into the chamber at 450 K (CH<sub>4</sub>/O<sub>2</sub> reaction feed), no changes were seen in the C 1s XPS region for Cu<sub>2</sub>O/Cu(111) and CeO<sub>2</sub>/Cu<sub>2</sub>O/Cu(111) surfaces. In particular, no CH<sub>3</sub>O peak around 286.5 eV was detected. This result is consistent with the lack of CH<sub>3</sub>OH formation over these surfaces where only CO and CO<sub>2</sub> are detected as reaction products in the absence of H<sub>2</sub>O (16). Although O<sub>2</sub> dissociates readily on CeO<sub>x</sub>/Cu<sub>2</sub>O/Cu(111) (23), a metal-O or metal=O group is not an efficient agent for the formation of CH<sub>3</sub>OH on these surfaces. A CH<sub>3</sub>O intermediate could be formed, but it probably would decompose very rapidly on some active sites of the surface (see DFT calculations below) producing mainly CO/CO<sub>2</sub> and not give a signal in AP-XPS (16).

The addition of H<sub>2</sub>O to the CH<sub>4</sub>/O<sub>2</sub> reaction mixture induced drastic changes in the chemical process. On CeO<sub>2</sub>/Cu<sub>2</sub>O/Cu(111), water dissociated to form OH on the surface at 300 and 450 K as seen in AP-XPS (Fig. S1). Signals for OH species bound to Cu<sub>2</sub>O (~531.1 eV) (15) and ceria (~532.1 eV) (21) were observed in the O 1s region (Fig. S1). Fig. 2A shows C 1s XPS spectra collected while exposing a CeO<sub>2</sub>/Cu<sub>2</sub>O/Cu(111) surface ( $\theta_{\text{CeO}_2} = 0.5$ ) to a set of CH<sub>4</sub>/O<sub>2</sub>/H<sub>2</sub>O reactants at temperatures between 300 and 450 K. In the presence of water, one can see a clear change in the C 1s features with signals not seen in the case of a dry experiment, where only moderate amounts of CH<sub>x</sub> and CO<sub>x</sub> are detected (for an example, see Fig. 1A). The spectra in Fig. 2A were curve fitted (Fig. S2) well with peaks for CO<sub>x,ads</sub>, CH<sub>4,gas</sub>, CH<sub>3</sub>O<sub>ads</sub>, CH<sub>x,ads</sub> and C<sub>ads</sub> (24). In test experiments for the adsorption of CH<sub>3</sub>OH and its derivatives, the features around 286.2 eV corresponded to adsorbed CH<sub>3</sub>O, in good agreement with previous XPS studies (25, 26). As mentioned above, this species was not seen after exposing the surfaces to a simple CH<sub>4</sub>/O<sub>2</sub> reaction mixture. Furthermore, in Fig. 2A, the adsorbed CH<sub>3</sub>O was seen at temperatures of 400 and 450 K, which were the onset for a catalytic CH<sub>4</sub>→CH<sub>3</sub>OH transformation over CeO<sub>2</sub>/Cu<sub>2</sub>O/Cu(111) surfaces exposed to a mixture of CH<sub>4</sub>/O<sub>2</sub>/H<sub>2</sub>O (16).

Figure 2B compares C 1s spectra collected after exposing a CeO<sub>2</sub>/Cu<sub>2</sub>O/Cu(111) surface ( $\theta_{\text{CeO}_2} = 0.5$ ) to CH<sub>4</sub>, CH<sub>4</sub> + O<sub>2</sub>, CH<sub>4</sub> + H<sub>2</sub>O, and CH<sub>4</sub> + H<sub>2</sub>O + O<sub>2</sub> at 450 K, a threshold for CH<sub>3</sub>OH production (16). The amounts of CH<sub>x</sub> and CH<sub>3</sub>O present on the catalyst surface under pure CH<sub>4</sub> and a CH<sub>4</sub>/O<sub>2</sub> mixture were negligible. Thus, a reaction feed of CH<sub>4</sub>/O<sub>2</sub> produced mainly (~95%) CO and CO<sub>2</sub> as products (16). CH<sub>3</sub>O and CH<sub>x</sub> appeared when H<sub>2</sub>O is added to the reaction feed, but the amount of CH<sub>3</sub>O was larger when a mixture of CH<sub>4</sub>/O<sub>2</sub>/H<sub>2</sub>O is used (Fig. S3), and the CH<sub>3</sub>O signal in AP-XPS was correlated with the CH<sub>3</sub>OH selectivity measured in catalytic tests (Fig. 2C). At high temperatures, CH<sub>4</sub> alone could induce a partial reduction of the ceria overlayer (Fig. S4), but under a mixture of CH<sub>4</sub>/O<sub>2</sub>/H<sub>2</sub>O, the ceria remained fully oxidized (Fig. S5). And

there was not reduction of the Cu<sub>2</sub>O film in between ceria and Cu(111). Although the CeO<sub>2</sub>/Cu<sub>2</sub>O/Cu(111) system has special properties for the dissociation of CH<sub>4</sub> (Fig. 1), some of its sites were probably too reactive to allow any CH<sub>3</sub>O formed to avoid decomposition. The OH groups coming from water dissociation (22) were necessary to block these sites and, as we will see below, they also could participate in an additional reaction path for the activation and conversion of CH<sub>4</sub>.

Our AP-XPS measurements were fully consistent with the theoretical calculations using DFT and the KMC simulation under the experimental conditions (pressure ratio: CH<sub>4</sub> : O<sub>2</sub> = 2:1 or CH<sub>4</sub> : O<sub>2</sub> : H<sub>2</sub>O = 2: 1 : 8; T= 450K, see SI for details). In the DFT calculations, the CeO<sub>2</sub>/Cu<sub>2</sub>O/Cu(111) catalyst was modeled by depositing a Ce<sub>3</sub>O<sub>6</sub> cluster on the 44 structure of Cu<sub>2</sub>O/Cu(111) (Fig. S6A, see SI for detail and (16). [note referee comment about the cluster used] According to the DFT results, the CeO<sub>2</sub>/Cu<sub>2</sub>O/Cu(111) system should produce mainly CO<sub>2</sub> from a CH<sub>4</sub>/O<sub>2</sub> mixture following a reaction path that is highly exothermic (Fig. S7 and S8). Initially, upon exposure to CH<sub>4</sub> and O<sub>2</sub>, an active Ce site (Ce-2 in Fig.S6B) at the CeO<sub>2</sub>-Cu<sub>2</sub>O/Cu(111) interface stabilized O<sub>2</sub> (binding energy or E<sub>ads</sub> = -14.53 kcal/mol) [given the expts are in kcal/mol, it would be better to report the energies the same way here] and enabled the facile O-O bond cleavage with the synergy of Cu from the Cu<sub>2</sub>O film (reaction energy or ΔE = -24.44 kcal/mol; activation barrier or E<sub>a</sub> = 5.54 kcal/mol, Fig. 3A). However, in this case, none of the terminal metal=O oxo ligands, which were previously proposed as the active sites for CH<sub>4</sub> to CH<sub>3</sub>OH conversion for the zeolite-based systems (10, 17-19), survived. Instead, the doubly bridging oxo ligand formed (\*O) over the interfacial Cu-Ce bridge sites (Fig. 3A and S7).

The CH<sub>4</sub> also preferred the same Ce site; yet the KMC simulations show that it could not compete with O<sub>2</sub> because of weakened binding (E<sub>ads</sub> = -2.54 kcal/mol) and the elevated barrier for dissociation (E<sub>a</sub> = 11.76 kcal/mol) (16). Thus, all active Ce sites at the CeO<sub>2</sub>/Cu<sub>2</sub>O/Cu(111) were occupied by \*O from O<sub>2</sub> dissociation. The formed doubly bridging oxo Ce-O-Cu species were active to adsorb (E<sub>ads</sub> = -1.15 kcal/mol) and activate CH<sub>4</sub> through the preferential C-O bond association. Either methoxy (\*CH<sub>3</sub>O) species (ΔE = -37.82 kcal/mol, E<sub>a</sub> = 18.45 kcal/mol, Fig. S7 and S8) formed, or \*CH<sub>3</sub>OH formed directly at the interface (E<sub>a</sub> = 16.37 kcal/mol). The KMC simulations, however, demonstrated that the produced \*CH<sub>3</sub>OH was not stable and preferentially dissociated to \*CH<sub>3</sub>O with no barrier (ΔE = -14.53 kcal/mol).

The sequential dehydrogenation of \*CH<sub>3</sub>O to \*CH<sub>2</sub>O, \*CHO and eventually production of CO<sub>2</sub> was highly favorable in terms of both thermodynamics and kinetics according to the DFT calculations (Fig. S7), and hence none of the intermediates was likely to be stable. Indeed, under steady states the CeO<sub>2</sub>/Cu<sub>2</sub>O/Cu(111) surface remained clean on exposure to CH<sub>4</sub> and O<sub>2</sub>, as demonstrated by the KMC snapshot (Fig. S9). No \*CH<sub>3</sub>O or other adsorbed surface species could be observed, which agreed well with the AP-XPS measurements in Fig. 2B and 2C for the experiment with a CH<sub>4</sub>/O<sub>2</sub> reaction feed. Regarding the products in the catalytic tests (16), the KMC results were consistent with the experimental results (Fig. 2C), showing that CeO<sub>2</sub>/Cu<sub>2</sub>O/Cu(111) was highly selective to CO<sub>2</sub>/CO on exposure to CH<sub>4</sub> and O<sub>2</sub> rather than CH<sub>3</sub>OH (Fig. 4A). Finally, during the dehydrogenation process, oxygen vacancies (O<sub>v</sub>, Fig. S7 and Fig. S8) were generated on the supported CeO<sub>2</sub> cluster, that could be quickly filled in presence of O<sub>2</sub> as reported previously (16).

The addition of H<sub>2</sub>O in the mixture of CH<sub>4</sub> and O<sub>2</sub> changed the reaction network on the catalyst surface. First, H<sub>2</sub>O blocked the adsorptions and dissociation of O<sub>2</sub> at the active interfacial Ce site (Fig. 3A), as seen under exposure of CH<sub>4</sub> and O<sub>2</sub>. According to the DFT calculations, H<sub>2</sub>O



also preferred ( $E_{\text{ads}} = -15.91$  kcal/mol), as did  $\text{O}_2$ , to adopt a tilted conformation [please check my edit, but the original was not clear, and picking out one structure in fig S9 and S10 is not obvious] because of the formation of hydrogen bond with nearby bridging oxygen (Fig. 3A, S10 and S11). The tilted adsorption was followed by a spontaneous O-H bond cleavage (Fig. 3A), which was much more facile than the O-O ( $E_a = 5.54$  kcal/mol) and C-H bond breakage ( $E_a = 11.76$  kcal/mol) (16). Also, the pressure of  $\text{H}_2\text{O}$  was eight times higher than that of  $\text{O}_2$  under reaction conditions considered in both experiment and KMC simulations. Thus [the next sentence on adsorption doesn't follow in an obvious way—did the KMC sims also use this pressure ratio?], the KMC simulations showed that the adsorption rate of  $\text{O}_2$  decreased by a factor of  $\sim 30$  by the addition of  $\text{H}_2\text{O}$ . In this case, 90% of active Ce sites were occupied by hydroxyl ( $^*\text{OH}$ ) from  $\text{H}_2\text{O}$  dissociation and only 10% formed the Ce-O-Cu oxo species, as was the case without  $\text{H}_2\text{O}$ . Thus, the adsorbed  $^*\text{OH}$  groups blocked reactive Ce sites from interaction with  $\text{O}_2$  and in the presence of  $\text{H}_2\text{O}$ , new reaction paths are enabled to facilitate  $\text{CH}_3\text{OH}$  production ( Fig. 3A, S10 and S11).

The  $^*\text{OH}$  species generated by  $\text{H}_2\text{O}$  dissociation at the interfacial Ce sites opened a new highly effective pathway for a real catalytic transformation (Fig. 3B and S10). Along the new path, the direct conversion from  $\text{CH}_4$  to  $^*\text{CH}_3\text{OH}$  is substantially populated by the active  $^*\text{OH}$  at the Ce site (Fig. 3B and S10) through the concerted C-O bond association and C-H dissociation ( $\Delta E = -18.68$  kcal/mol,  $E_a = 22.37$  kcal/mol). This step represented the rate-limiting step along the path and the negative shift in barrier by 0.1 eV can effectively increase the  $\text{CH}_4$  conversion by 93.79% and  $\text{CH}_3\text{OH}$  selectivity by 3.78%. This reaction is followed by the barrierless dissociation to  $^*\text{CH}_3\text{O}$ , as was for the  $\text{CH}_4$  oxidation by  $\text{O}_2$ . The difference is that the presence of  $\text{H}_2\text{O}$  predominantly blocked the  $^*\text{CH}_3\text{O}$  decomposition and thus the formation of  $\text{CO}_2$ . Instead,  $\text{H}_2\text{O}$  also enabled the extraction of  $\text{CH}_3\text{OH}$  from  $^*\text{CH}_3\text{O}$ , or the removal of  $^*\text{CH}_3\text{O}$  as gas phase  $\text{CH}_3\text{OH}$ , in addition to blocking  $\text{O}_2$  adsorption and activating  $\text{CH}_4$ .

This process started with the formation of  $^*\text{CH}_3\text{O}\cdots\text{HOH}$  through hydrogen bonding (Fig. 3C and S12). This structural motif drove the proton hopping from  $\text{H}_2\text{O}$  to  $^*\text{CH}_3\text{O}$  ( $\Delta E = 4.85$  kcal/mol,  $E_a = 6.69$  kcal/mol, Fig. 3C and S12) and produces gas phase  $\text{CH}_3\text{OH}$  and the active  $^*\text{OH}$  to replace the binding site for  $^*\text{CH}_3\text{O}$  at interfacial Ce site, which is active for direct  $\text{CH}_4 \rightarrow \text{CH}_3\text{OH}$  conversion (Fig. 3B and S10). The dissociated  $^*\text{H}$  from  $\text{CH}_4$  resulted in the hydroxylation of  $\text{CeO}_2$  (Fig. S10 and S11), which could easily be removed with the assistance of  $^*\text{H}_2\text{O}$  at the Ce site, leading to the formation of oxygen vacancy ( $\text{O}_v$ ) and thus the reduced  $\text{CeO}_x$  ( $\Delta E = -8.30$  kcal/mol,  $E_a = 2.31$  kcal/mol, Fig. S10). At this point,  $\text{O}_2$  could preferentially fill the  $\text{O}_v$  and re-oxidize  $\text{CeO}_x$  to  $\text{CeO}_2$  (Fig. S10), which is the dominant role of  $\text{O}_2$  during this process due to the preferential  $\text{O}_2$  dissociation ( $E_a = 3.00$  kcal/mol) over  $\text{H}_2\text{O}$  dissociation ( $E_a = 15.45$  kcal/mol) at the  $\text{O}_v$  site.

According to the KMC simulations, under steady states of  $\text{CH}_4$  oxidation by  $\text{O}_2$  and  $\text{H}_2\text{O}$ , the  $\text{CeO}_2/\text{Cu}_2\text{O}/\text{Cu}(111)$  surface was not clean anymore. Instead, two stable surface species,  $^*\text{OH}$  and  $^*\text{CH}_3\text{O}$  (Fig. 4B), which agreed very well with measurements of AP-XPS (Fig. 2B). Both surface species bound to the supported  $\text{CeO}_2$  at the interface (Fig. S13). The formation of  $^*\text{OH}$  was associated with  $\text{H}_2\text{O}$  and  $\text{CH}_4$  dissociation, and  $^*\text{CH}_3\text{O}$  is formed because of the interplay between the barrierless O-H bond cleavage of  $^*\text{CH}_3\text{OH}$  and the activated extraction of  $\text{CH}_3\text{OH}$  from  $^*\text{CH}_3\text{O}$  by  $\text{H}_2\text{O}$  (Fig. 3C, S7 and S10).

The amount of  $^*\text{OH}$  present on the catalyst surface was larger than the amount of  $^*\text{CH}_3\text{O}$  (Fig 4B), a condition which was essential to prevent the full oxidation of the formed  $^*\text{CH}_3\text{O}$

species. The stabilized  $^*\text{CH}_3\text{O}$  and the enabled  $^*\text{CH}_3\text{O}$  extraction by adding of  $\text{H}_2\text{O}$  to the mixture of  $\text{CH}_4$  and  $\text{O}_2$  tuned the selectivity of  $\text{CeO}_2/\text{Cu}_2\text{O}/\text{Cu}(111)$  from  $\text{CO}_2$  to  $\text{CH}_3\text{OH}$  as the major product according to the KMC simulations (Fig. 4A), which was also observed by the AP-XPS measurements and catalytic tests [Fig. 2C and (16)]. The addition of  $\text{H}_2\text{O}$  also facilitated the  $\text{CH}_3\text{OH}$  production through oxidation of  $\text{CH}_4$  by  $\text{O}_2$  by hindering the  $^*\text{CH}_3\text{O}$  dehydrogenation and promoting the extraction of  $\text{CH}_3\text{OH}$  according to the KMC simulation results (Fig. 3C and S13). About one half of the dissociated  $^*\text{O}$  at the active Ce sites led to the  $\text{CH}_3\text{OH}$  production, and the rest remained as oxidizing agent to produce  $\text{CO}_2$ . Yet, because of lower adsorption rate of  $\text{O}_2$  than  $\text{H}_2\text{O}$  at the active Ce sites, 95% of produced  $\text{CH}_3\text{OH}$  is by reaction with  $\text{H}_2\text{O}$ , and the dominant roles that  $\text{O}_2$  plays is to fill the  $\text{O}_v$  sites via facile dissociation. [as meant?  $\text{O}_2$  just reoxidizes Ce]

The AP-XPS data were consistent with the results of combined DFT and KMC simulations, showing that on the active  $\text{CeO}_2\text{-Cu}_2\text{O}$  interfaces,  $\text{CH}_4$  was preferentially oxidized by  $\text{O}_2$  into  $\text{CO}$  and  $\text{CO}_2$  (Fig. S14A). When  $\text{H}_2\text{O}$  is added to a  $\text{CH}_4/\text{O}_2$  mixture, the selectivity was tuned toward  $\text{CH}_3\text{OH}$  (Fig. S14B). The  $\text{CeO}_2/\text{Cu}_2\text{O}/\text{Cu}(111)$  inverse catalyst exhibited a reactivity different from that reported for zeolite-based materials during the selective oxidation of  $\text{CH}_4$ . On the zeolite-based catalysts,  $\text{O}_2$  is considered as the oxidizing agent and  $\text{H}_2\text{O}$  is just extracting [there has to be a better word—displacing?] the formed  $^*\text{CH}_3\text{OH}$ .

However, on  $\text{CeO}_2/\text{Cu}_2\text{O}/\text{Cu}(111)$ ,  $\text{H}_2\text{O}$  played three key roles. As on a zeolite-based material,  $\text{H}_2\text{O}$  acted as a site blocker. It preferentially occupied the active Ce sites at the  $\text{CeO}_2\text{-Cu}_2\text{O}$  interface, which hindered the  $\text{O}_2$  activation and thus the conversion of  $\text{CH}_4$  to  $\text{CO}$  or  $\text{CO}_2$  (Fig.3A). More importantly, it was an active center, where the facial dissociation at the interfacial Ce sites produced the active  $^*\text{OH}$ , being able to open a new pathway and promote the direct  $\text{CH}_4$  to  $\text{CH}_3\text{OH}$  conversion (Fig.3B). In this case,  $\text{H}_2\text{O}$  participated in the reaction directly as the actual O-provider and enables the direct  $\text{CH}_4$  to  $\text{CH}_3\text{OH}$  conversion. In this system,  $\text{O}_2$  only helped to re-oxidize  $\text{CeO}_x$ , which was partially reduced during the reaction. Finally,  $\text{H}_2\text{O}$  functioned as an extractor as proposed previously, preventing the dehydrogenation of  $^*\text{CH}_3\text{O}$  and thus  $\text{CO}_2$  formation, while facilitating the hydrogenation and thus  $\text{CH}_3\text{OH}$  formation (Fig.3C). The identification of the key roles played by  $\text{H}_2\text{O}$  while tuning the selectivity during  $\text{CH}_4$  conversion points to phenomena that must be taken into consideration when dealing with new routes for designing efficient catalyst for the selective  $\text{CH}_4 \rightarrow \text{CH}_3\text{OH}$  oxidation.

## References and Notes:

1. A. C. Rosenzweig, C. A. Frederick, S. J. Lippard, P. Nordlund, Crystal structure of a bacterial non-haem iron hydroxylase that catalyses the biological oxidation of methane. *Nature* **366**, 537-543 (1993).
2. S. Sirajuddin, A. C. Rosenzweig, Enzymatic oxidation of methane. *Biochemistry* **54**, 2283-2294 (2015).
3. M. O. Ross, F. MacMillan, J. Wang, A. Nisthal, T. J. Lawton, B. D. Olafson, S. L. Mayo, A. C. Rosenzweig, B. M. Hoffman, Particulate methane monooxygenase contains only mononuclear copper centers. *Science* **364**, 566-570 (2019).
4. R. Balasubramanian S. M. Smith, S. Rawat, L. A. Yatsunyk, T. L. Stemmler, A. C. Rosenzweig, Oxidation of methane by a biological dicopper centre. *Nature* **465**, 115-119 (2010).

5. M. Ravi, M. Ranocchiari, A. van Bokhoven Jeroen, The direct catalytic oxidation of methane to methanol - A critical assessment. *Angew. Chem. Int. Ed.* **56**, 16464-16483 (2017).
6. V. L. Sushkevich, D. Palagin, M. Ranocchiari, J. A. van Bokhoven, Selective anaerobic oxidation of methane enables direct synthesis of methanol. *Science* **356**, 523-527 (2017).
7. S. Grundner, M. A. Markovits, G. Li, M. Tromp, E. A. Pidko, E. J. Hensen, A. Jentys, M. Sanchez-Sanchez, J. A. Lercher, Single-site trinuclear copper oxygen clusters in mordenite for selective conversion of methane to methanol. *Nat. Commun.* **6**, 7546 (2015).
8. J. Shan, M. Li, L. F. Allard, S. Lee, M. Flytzani-Stephanopoulos, Mild oxidation of methane to methanol or acetic acid on supported isolated rhodium catalysts. *Nature* **551**, 605-608 (2017).
9. C. Hammond, M. M. Forde, M. H. Ab Rahim, A. Thetford, Q. He, R. L. Jenkins, N. Dimitratos, J. A. Lopez-Sanchez, N. F. Dummer, D. M. Murphy, A. F. Carley, S. H. Taylor, D. J. Willock, E. E. Stangland, J. Kang, H. Hagen, C. J. Kiely, G. J. Hutchings, Direct catalytic conversion of methane to methanol in an aqueous medium by using copper-promoted Fe-ZSM-5. *Angew. Chem. Int. Ed.* **51**, 5129-5133 (2012).
10. M. H. Groothaert, P. J. Smeets, B. F. Sels, P. A. Jacobs, R. A. Schoonheydt, Selective oxidation of methane by the bis ( $\mu$ -oxo) dicopper core stabilized on ZSM-5 and mordenite zeolites. *J. Am. Chem. Soc.* **127**, 1394-1395 (2005).
11. P. Tomkins, A. Mansouri, S. E. Bozbag, F. Krumeich, M. B. Park, E. M. C. Alayon, M. Ranocchiari, J. A. van Bokhoven, Isothermal cyclic conversion of methane into methanol over copper-exchanged zeolite at low temperature. *Angew. Chem. Int. Ed.* **55**, 5467-5471 (2016).
12. Z. Liang, T. Li, M. Kim, A. Asthagiri, J. F. Weaver, Low-temperature activation of methane on the IrO<sub>2</sub> (110) surface. *Science* **356**, 299-303 (2017).
13. Z. Liu, P. Lustemberg, R. A. Gutierrez, J. J. Carey, R. M. Palomino, M. Vorokhta, D. C. Grinter, D. C.; P. J. Ramirez, V. Matolin, M. Nolan, M. V. Ganduglia-Pirovano, S. D. Senanayake, J. A. Rodriguez, In-situ investigation of methane dry reforming on metal/ceria(111) surfaces: Metal-support interactions and C-H bond activation at low temperature. *Angew. Chem. Int. Ed.* **56**, 13041-13046 (2017).
14. P. G. Lustemberg, R. M. Palomino, R. A. Gutierrez, D. C. Grinter, M. Vorokhta, Z. Liu, P. J. Ramirez, V. Matolin, M. V. Ganduglia-Pirovano, S. D. Senanayake, J. A. Rodriguez, Direct conversion of methane to methanol on Ni-ceria surfaces: Metal-support interactions and water-enabled catalytic conversion by site blocking. *J. Am. Chem. Soc.* **140**, 7681-7687 (2018).
15. X. Deng, T. Herranz, C. Weis, H. Bluhm, M. Salmeron, Adsorption of water on Cu<sub>2</sub>O and Al<sub>2</sub>O<sub>3</sub> thin films. *J. Phys. Chem. C* **112**, 9668-9672 (2008).
16. Z. Zuo, P. J. Ramirez, S. D. Senanayake, P. Liu, J. A. Rodriguez, Low-temperature conversion of methane to methanol on CeO<sub>x</sub>/Cu<sub>2</sub>O catalysts: water controlled activation of the C-H bond. *J. Am. Chem. Soc.* **138**, 13810-13813 (2016).
17. P. J. Smeets, R. G. Hadt, J. S. Woertink, P. Vanelderen, R. A. Schoonheydt, B. F. Sels, E. I. Solomon, Oxygen precursor to the reactive intermediate in methanol synthesis by Cu-ZSM-5. *J. Am. Chem. Soc.* **132**, 14736-14738 (2010).

18. J. S. Woertink, P. J. Smeets, M. H. Groothaert, M. A. Vance, B. F. Sels, R. A. Schoonheydt, E. I. Solomon, A  $[\text{Cu}_2\text{O}]^{2+}$  core in Cu-ZSM-5, the active site in the oxidation of methane to methanol. *Proc. Natl. Acad. Sci. U.S.A.* **106**, 18908-18913 (2009).
19. G. Li, P. Vassilev, M. Sanchez-Sanchez, J. A. Lercher, E. J. M. Hensen, E. A. Pidko, Stability and reactivity of copper oxo-clusters in ZSM-5 zeolite for selective methane oxidation to methanol. *J. Catal.* **338**, 305-312 (2016).
20. P. Tomkins, M. Ranocchiari, J. A. van Bokhoven, Direct conversion of methane to methanol under mild conditions over Cu-zeolites and beyond. *Acc. Chem. Res.* **50**, 418-425 (2017).
21. J. Carrasco, D. López-Durán, Z. Liu, T. Duchoň, J. Evans, S. D. Senanayake, E. J. Crumlin, V. Matolín, J. A. Rodríguez, M. V. Ganduglia-Pirovano, In situ and theoretical studies for the dissociation of water on an active Ni/CeO<sub>2</sub> catalyst: Importance of strong metal-support interactions for the cleavage of O–H bonds. *Angew. Chem. Int. Ed.* **54**, 3917-3921 (2015).
22. J. A. Rodríguez, J. Graciani, J. Evans, J. B. Park, F. Yang, D. Stacchiola, S. D. Senanayake, S. Ma, M. Pérez, P. Liu, J. F. Sanz, J. Hrbek, Water-gas shift reaction on a highly active inverse CeO<sub>x</sub>/Cu(111) Catalyst: Unique role of ceria nanoparticles. *Angew. Chem. Int. Ed.* **48**, 8047-8050 (2009).
23. F. Yang, J. Graciani, J. Evans, P. Liu, J. Hrbek, J. F. Sanz, J. A. Rodríguez, CO oxidation on inverse CeO<sub>x</sub>/Cu(111) catalysts: High catalytic activity and ceria-promoted dissociation of O<sub>2</sub>. *J. Am. Chem. Soc.* **133**, 3444-3451 (2011).
24. Y. Lykhach, T. Staudt, M. P. A. Lorenz, R. Streber, A. Bayer, H.-P. Steinrück, J. Libuda, Microscopic insights into methane activation and related processes on Pt/ceria model catalysts. *ChemPhysChem* **11**, 1496-1504 (2010).
25. A. Siokou, R. M. Nix, Interaction of methanol with well-defined ceria surfaces: Reflection/absorption infrared spectroscopy, X-ray photoelectron spectroscopy, and temperature-programmed desorption study. *J. Phys. Chem. B* **103**, 6984-6997 (1999).
26. D. R. Mullins, Variations in the surface chemistry of methanol with CeO<sub>2</sub>(100) at low and elevated pressures. *Surf. Interface Anal.* **50**, 913-920 (2018).
27. G. Kresse, J. Furthmüller, Efficiency of ab-initio total energy calculations for metals and semiconductors using a plane-wave basis set. *Comput. Mater. Sci.* **6**, 15-50 (1996).
28. C. T. Campbell, L. Árnadóttir, J. R. V. Sellers, Kinetic prefactors of reactions on solid surfaces. *Z. Phys. Chem.* **227**, 1435-1454 (2013).
29. S. Kattel, P. J. Ramírez, J. G. Chen, J. A. Rodríguez, P. Liu, Active sites for CO<sub>2</sub> hydrogenation to methanol on Cu/ZnO catalysts. *Science* **355**, 1296-1299 (2017).
30. NIST computational chemistry comparison and benchmark database. <http://cccbdb.nist.gov/>.

Refs 26 to 44 appear in this list and NOT in the SM, thx

### Acknowledgments:

**Funding:** The research carried out at Brookhaven National Laboratory (BNL), was supported by the U.S. Department of Energy, Office of Science and Office of Basic Energy Sciences under contract No. DE-SC0012704. X-ray spectroscopy measurements were performed at beamline 9.3.2 at the Advanced Light Source of LBNL, which is a DOE Office of Science User Facility under



contract no. DE-AC02-05CH11231. The DFT calculations were performed using computational resources at the Center for Functional Nanomaterials, a U.S. DOE Office of Science Facility, and the Scientific Data and Computing Center, a component of the Computational Science Initiative at BNL under Contract No. DE-SC0012704, at the National Energy Research Scientific Computing Center (NERSC), a DOE Office of Science User Facility, supported by the Office of Science of the DOE under contract DE-AC02-05CH11231 and at Stony Brook University, which was founded by National Science Foundation grant (#1531492). SDS is partially supported by a U.S. DOE Early Career Award. **Author contributions:** P.L., J.A.R. and S.D.S. came with the general idea and supervised the execution of the project and written of the article. Z.L and E.H. worked in the main writing of the manuscript. Z.L., R.M.P., T.D., S.N. and D.C.G. performed synchrotron photoemission experiments at the ALS. I.O., N.R. and M.M. did studies with XPS and morphology characterization. E.H and W.L. performed the theoretical calculations. **Competing interests:** The authors declare no competing financial interests. **Data and materials availability:** All data is available in the main text or the supplementary materials.

## Supplementary Materials:

Materials and Methods

Figures S1-S13

Tables S1-S2

References (27-30)

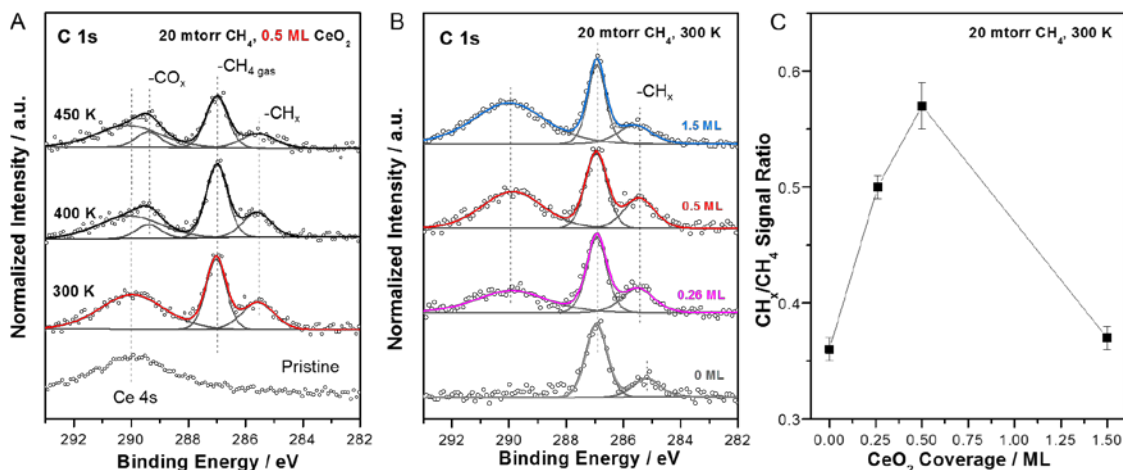


**Fig. 1. Methane interaction with CeO<sub>2</sub>/Cu<sub>2</sub>O/Cu(111).** C 1s region of the AP-XPS spectra for introducing 20 mTorr of CH<sub>4</sub> to (A) 0.5 ML CeO<sub>2</sub> covered Cu<sub>2</sub>O/Cu(111) surface at different temperatures, (B) different coverages of ceria on Cu<sub>2</sub>O/Cu(111) surface at 300 K. (C) Comparison

of the surface  $-\text{CH}_x$  amount derived from the integration of the corresponding C 1s normalized peak in (B).

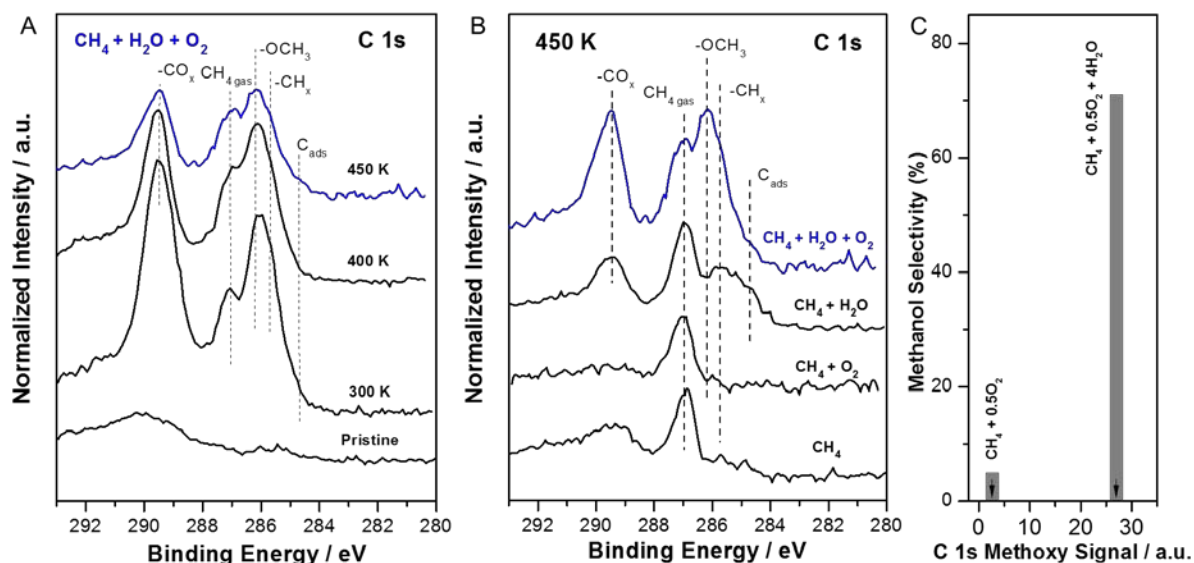
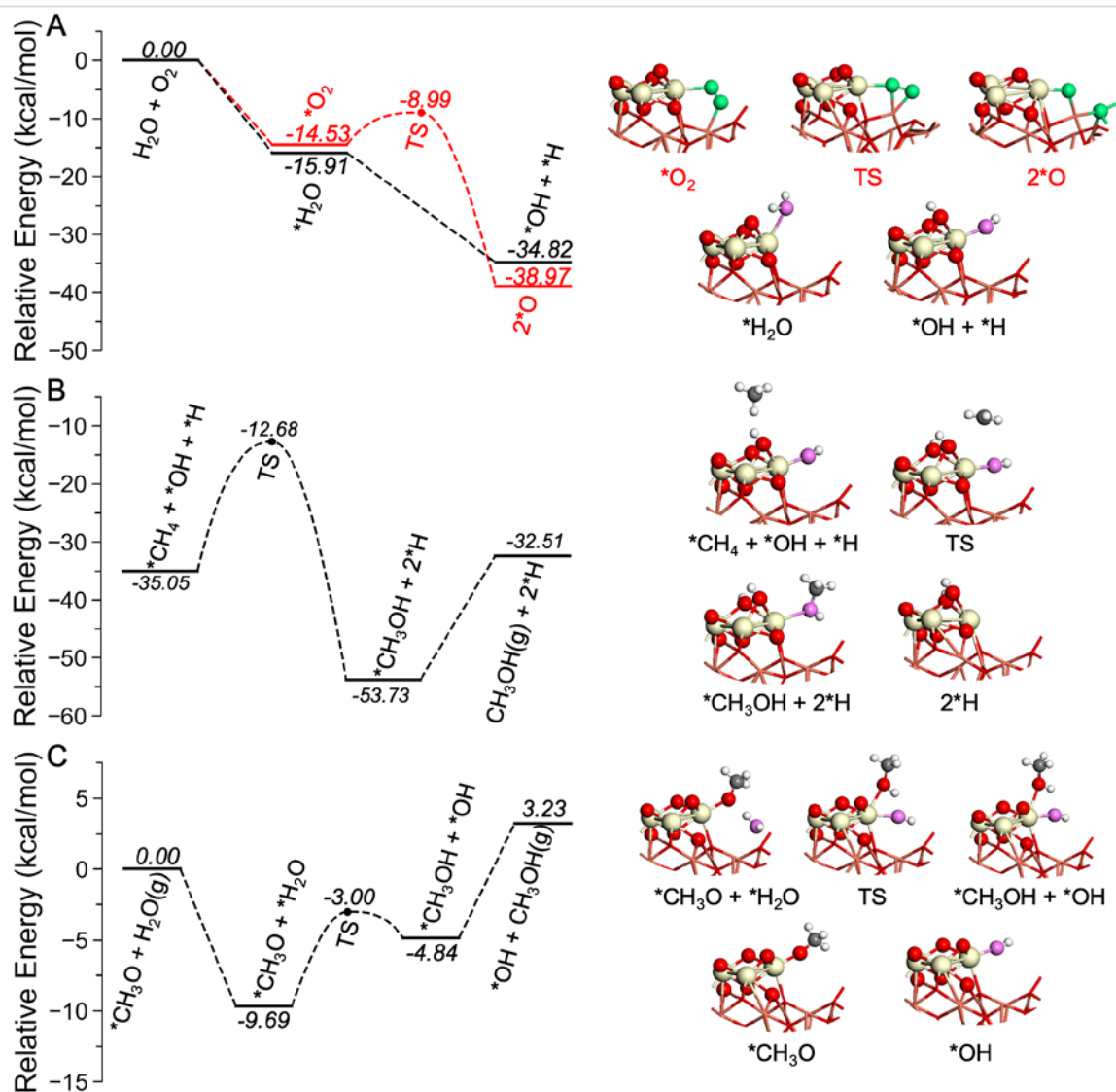


**Fig. 2. Water effects on methoxy formation on  $\text{CeO}_2/\text{Cu}_2\text{O}/\text{Cu}(111)$ .** C 1s region of the AP-XPS spectra for (A) the  $\text{CeO}_2/\text{Cu}_2\text{O}/\text{Cu}(111)$  surface ( $\theta_{\text{CeO}_2} \sim 0.5$  ML) when exposed to a 20 mTorr  $\text{CH}_4 + 80$  mTorr  $\text{H}_2\text{O} + 10$  mTorr  $\text{O}_2$  of gas mixture at different temperatures, (B) comparison of exposing  $\text{CeO}_2/\text{Cu}_2\text{O}/\text{Cu}(111)$  surfaces ( $\theta_{\text{CeO}_2} \sim 0.5$  ML) to different gas reactants at 450 K. (C)  $\text{CH}_3\text{OH}$

selectivity versus the amount of  $-\text{CH}_3\text{O}$  generated with and without addition of water. The results for the catalytic tests were taken from. (16).



As the referee noted, this is not very accessible – some heading in the figure, telling what is happening (absorption, what bond breaks or forms, etc) would help. It's not clear that all of the intermediates here are needed, as it's difficult to focus on key steps. The three roles of water should be clearly indicated as well. Also give the energy in kcal/mole on an axis on the right sides

**Fig. 3.** DFT-calculated potential energy diagrams for the three important steps involved in  $\text{CH}_4$  oxidation by  $\text{O}_2$  and  $\text{H}_2\text{O}$  on  $\text{CeO}_2/\text{Cu}_2\text{O}/\text{Cu}(111)$ . (A)  $\text{O}_2$  and  $\text{H}_2\text{O}$  dissociation, showing the preferential  $\text{H}_2\text{O}$  dissociative adsorption and thus the blocked active Ce sites from  $\text{O}_2$  by  $\text{H}_2\text{O}$ ; (B)  $\text{CH}_4$  oxidation by  $^*\text{OH}$ , demonstrating the enabled one-step  $\text{CH}_3\text{OH}$  synthesis from  $\text{CH}_4$  by dissociated fragments from  $\text{H}_2\text{O}$ ; (C) Hydrogenation of  $^*\text{CH}_3\text{O}$  by  $\text{H}_2\text{O}$ , indicating the facilitated  $\text{CH}_3\text{OH}$  formation or extraction by  $\text{H}_2\text{O}$ . The structures of intermediates and transition states (TS)

were also included. Yellow: Ce; brown: Cu; red: O in CeO<sub>2</sub>/Cu<sub>2</sub>O/Cu(111) (A) and \*CH<sub>x</sub>O (B); green: O in O<sub>2</sub>; purple: O in H<sub>2</sub>O; gray: C; white: H.

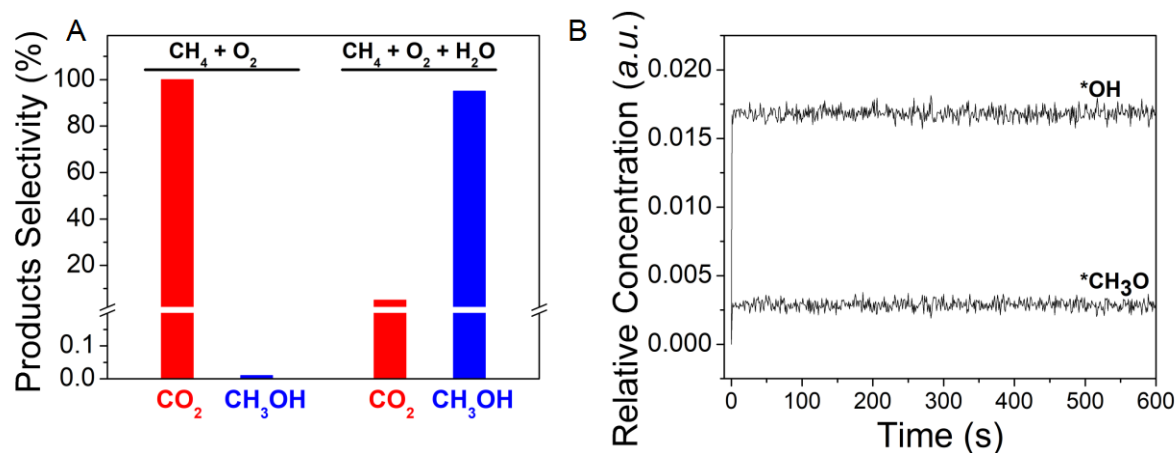


**Fig. 4. KMC-simulated product selectivity and reaction intermediates.** (A) Selectivity of CH<sub>4</sub> oxidation over CeO<sub>2</sub>/Cu<sub>2</sub>O/Cu(111) on exposure to CH<sub>4</sub> and O<sub>2</sub> with pressure ratio of 2:1 or CH<sub>4</sub>, O<sub>2</sub> and H<sub>2</sub>O with pressure ratio of 2:1:8 at 450K. (B) Coverage of adsorbed surface species on CeO<sub>2</sub>/Cu<sub>2</sub>O/Cu(111) under the mixture of CH<sub>4</sub>, O<sub>2</sub> and H<sub>2</sub>O.